Strong-field-induced Coulomb Explosion Imaging of Tribromomethane

Surjendu Bhattacharyya, Kurtis Borne, Farzaneh Ziaee, Shashank Pathak, Enliang Wang, Anbu Selvam Venkatachalam, Xiang Li[+], Nathan Marshall, Kevin D. Carnes, Charles W. Fehrenbach, Travis Severt, Itzik Ben-Itzhak, Artem Rudenko and Daniel Rolles*

J. R. Macdonald Laboratory, Department of Physics, Kansas State University, Manhattan, KS 66506, USA

[+]*current address: LCLS,* SLAC National Accelerator Laboratory, Menlo Park, CA 94025, USA

*Corresponding Author: *E-mail*: **rolles@phys.ksu.edu**

Abstract: The Coulomb explosion of tribromomethane ($CHBr_3$) induced by 28-femtosecond near-infrared laser pulses is investigated by three-dimensional coincidence ion momentum imaging. We focus on the fragmentation into three, four, and five ionic fragments measured in coincidence and present different ways of visualizing the three-dimensional momentum correlations. We show that the experimentally observed momentum correlations for four-and five-fold coincidences are well reproduced by classical Coulomb explosion simulations and contain information on the structure of the parent molecule that could be used to differentiate structural isomers formed, e.g., in a pump-probe experiment. Our results thus provide a clear path towards visualizing structural dynamics in polyatomic molecules by strong-field induced Coulomb explosion imaging.

TOC Graphic

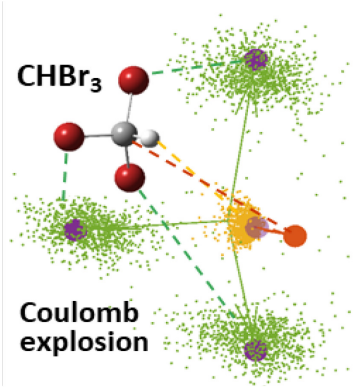

The advent of intense, high-repetition-rate light sources from the near-infrared to the X-ray regime has sparked renewed interest in multi-particle coincidence experiments to study ultrafast molecular dynamics in gas-phase molecular targets. One of the techniques discussed in this context is time-resolved Coulomb explosion imaging (CEI). Originally developed for (static) structure determination of dilute molecular beam targets,[1-5] CEI has found quite a number of different applications in recent years including identification of molecular isomers;[6-18] imaging of nuclear wavepackets in diatomic and triatomic molecules;[11, 19-22] and studies of fragmentation, dissociation, and isomerization reactions.[12-15, 23-31] However, with few exceptions, most CEI studies rely on the coincidence detection of no more than two or three ionic fragments. Detecting only two coincident ions necessarily limits the retrievable structural information to a single internuclear distance, while coincident detection of three ions can provide information on three variables, for example *two* distances and *one* molecular angle, albeit with some limitations.[32] More complete structural information for polyatomic molecules generally requires detection of more ionic fragments and thus significantly longer acquisition times due to limited detection efficiency and the relatively smaller yield of such highly charged final states. Therefore, time-resolved coincidence experiments detecting more than three particles are very rare to date. However, as high-power 100-kHz-repetition-rate near-infrared lasers and XFELs with repetition rates of tens of kHz to one MHz are becoming available, time-resolved coincidence experiments detecting four or more particles are now becoming a realistic scenario. As a first step, it is therefore crucial to develop a better understanding of four- and five-body Coulomb explosion patterns in general since only a few such experiments, even without time resolution, have been reported to date. In addition to pioneering CEI studies by Vager and coworkers on CH_4^+ and acetylene ion beams[2-4] , and more recently, also on more complex chiral targets,[33] Pitzer *et al.* used strong-field and X-ray induced Coulomb explosion to determine the absolute molecular stereochemistry of the chiral molecule bromochlorofluoromethane (CHBrClF) via the momentum correlations of four and five ions detected in coincidence.[6, 34-35] Four-body coincidence experiments were also reported for strong-field ionization of formaldehyde.[36] More recently, Li *et al.* obtained Coulomb explosion patterns for a complete fragmentation of CH_3I induced by an intense X-ray free-electron laser (XFEL) pulse at 2 keV photon energy and demonstrated that the full 3D equilibrium geometry of this prototypical

polyatomic system can be determined from the measured ion momenta with the help of a charge buildup model.[37] Similar XFEL-based coincidence experiments also produced impressive Coulomb explosion images of the molecular structure of iodopyridine and iodopyrazine.[38]

Here, we present the results of a three-, four-, and five-body Coulomb explosion imaging experiment on tribromomethane ($CHBr_3$) performed with 28-femtosecond near-infrared laser pulses using a three-dimensional coincidence ion momentum imaging technique (see Methods). $CHBr_3$ was chosen as a prototypical five-atom molecule that is of interest for time-resolved photochemistry studies, e.g., to shed light on the ultrafast reaction pathways that lead to formation of molecular bromine (Br_2) and hydrogen bromide (HBr). For the former, a roaming-mediated isomerization pathway has been suggested to occur after UV-excitation of $CHBr_3$ at 255 and 250 nm in both the liquid and gas phases, respectively.[39-40] This process involves the formation of transient BrCHBr–Br (*iso*-$CHBr_3$), i.e., a molecule in which the two bromine atoms are bound to each other instead of to the central carbon atom (see inset in **Figure 3**). Matrix isolation studies have characterized *iso*-$CHBr_3$ and its deuterated isotopologue by electronic spectroscopy.[41] However, the proposed ultrafast roaming pathway including the transient formation of *iso*-$CHBr_3$ was not been observed in a recent UV pump (266 nm)–extreme UV (XUV) probe femtosecond transient-absorption-spectroscopy experiment.[42]

In order to investigate the feasibility of CEI for distinguishing *iso*-$CHBr_3$ from the $CHBr_3$ parent molecule, along with the experimental results on $CHBr_3$, we shall present Coulomb explosion simulations of $CHBr_3$ and *iso*-$CHBr_3$ performed on their ground-state geometries in subsequent sections. Despite having a very different molecular geometry, the predicted Coulomb explosion patterns of the $CHBr_3$ and *iso*-$CHBr_3$ isomers are quite similar. Nonetheless, our model calculations predict subtle yet distinct differences that should be resolvable when the momenta of four or five fragment ions are measured in coincidence. Combining the Coulomb explosion imaging method presented here with a pump-probe scheme should, therefore, be well suited to study and confirm the isomer formation and possible roaming dynamics of gas-phase $CHBr_3$ on the femtosecond time scale.

The following discussion of the CEI results is focused on three particular fragmentation channels, namely the three-body breakup into $Br^+ + Br^+ + CHBr^+$, the four-body breakup into $CH^+ + Br^+ + Br^+ + Br^+$, and the five-body breakup into $H^+ + C^+ + Br^+ + Br^+ + Br^+$. In particular the latter two

channels promise to carry direct information about the geometry of the three bromine atoms in the molecule. We note that our conclusions drawn for those channels would equally apply to similar four- and five-body fragmentation channels with more highly charged bromine (or carbon) ions, but channels with higher charged fragments are produced with a significantly lower probability for the laser conditions applied here, and we, therefore, concentrate on the most abundant channels.

To identify the fragmentation channels of interest in the measured coincidence data, we use an extension of the usual photoion-photoion coincidence (PIPICO) plot, shown in **Figure 1**, in which the coincident-ion yield is plotted as a function of the time of flight of the first detected ion and the sum of the times of flight of the subsequently detected ions. In the figure, we zoom into the region of interest for the above coincidence channels. The non-coincident ion time-of-flight spectrum is shown in **Figure S1** in the Supporting information, and the full (unzoomed) coincidence plots are shown in **Figures S2**, **S5**, and **S7**. Due to momentum conservation, the coincidence events of interest appear as sharp diagonal lines with negative slopes in these figures. Owing to the almost equal natural abundance of ^{79}Br and ^{81}Br isotopes (the isotope abundance ratio is ^{79}Br / ^{81}Br =1.03), each of the above channels consist of six diagonal stripes (the four mixed-isotope channels are partially overlapping and appear as two more intense diagonal lines in the center) corresponding to the six possible combinations of the naturally occurring isotopes: $^{79}Br^+ + {}^{79}Br^+ + CH^{79}Br^+$, $^{79}Br^+ + {}^{79}Br^+ + CH^{81}Br^+$, $^{79}Br^+ + {}^{81}Br^+ + CH^{79}Br^+$, $^{79}Br^+ + {}^{81}Br^+ + CH^{81}Br^+$, $^{81}Br^+ + {}^{81}Br^+ + CH^{79}Br^+$, and $^{81}Br^+ + {}^{81}Br^+ + CH^{81}Br^+$ (and equivalently for the four-body and five-body cases in **Figure 1b and 1c**). We restrict the following data analysis to the channels with only ^{81}Br, which are separated the most from any background contributions (e.g. the $C^+ + Br^+ + Br^+ + Br^+$ channel, which appears as fainter diagonal lines in **Figure 1b**).

From the three-dimensional ion momentum imaging data recorded in our experiment, we can extract the kinetic energy release (KER) and kinetic energy (KE) distributions of the individual ions as shown in **Figures S3, S6**, and **S8**, which contain some information about internuclear distances and charge distributions in the molecule. More detailed structural information along with some information about the fragmentation dynamics is encoded in fragments' three-dimensional momentum correlations. For three-body coincidence experiments, these momentum correlations are often displayed as two-

dimensional "Newton plots"[26, 28, 43-46] as shown in **Figure 2**, and we will be using an extension of such plots to three-dimensions in the following to display the four- and five-body momentum correlations.

In a three-body Newton plot, one of the fragments is chosen as a reference, and the magnitude and direction of the momentum vectors of the two other fragments with respect to the reference fragment are displayed on the top and bottom halves of the plot. Most commonly, the fragment momenta are normalized such that the magnitude of the reference ion's momentum is one, and we follow this convention here. Note that this normalization is particularly useful when comparing the experimentally observed Newton plots with Coulomb explosion simulations, which often overestimate the fragments' kinetic energies, e.g. due to the non-Coulombic nature of the ionic potential energy surfaces in the Franck-Condon region[47-49], but accurately reproduce the angular features in the momentum correlation maps, as we show in the following.

In **Figure 2**, the momentum correlation of the three-body $Br^+ + Br^+ + CHBr^+$ channel is displayed with one of the Br^+ ions as the reference, whose momentum is pointing along the P_x direction, as indicated by the red arrow. The relative momenta of the other two fragment ions are plotted in the upper and lower half of the plot, respectively. This representation reveals three distinct features: a circular structure consisting of two slightly offset semicircles (marked by the thin blue semicircles), two localized maxima (marked by the blue star symbols), and a curved "tail" that starts at the position of the maxima and curves back to the circular structure. Based on the experience from previous work on three-body fragmentation dynamics, these features are clear signatures of competing concerted and sequential fragmentation pathways.[28, 43-46, 50] In particular, the circular structure can be assigned to a sequential fragmentation pathway. In this pathway, the transient $CHBr_3^{3+}$ ion first breaks into a $CHBr_2^{2+} + Br^+$ pair. In the second step, the $CHBr_2^{2+}$ di-cation breaks into $CHBr^+ + Br^+$ after a time delay that is larger than the rotational period of the $CHBr_2^{2+}$ fragment. If the reference ion happens to be the Br^+ emitted in the first step, a (semi-) circular structure will appear, while choosing the Br^+ emitted in the second step as a reference causes the tail structure.[50] Our analysis reveals no significant contribution from a breakup into a $CHBr^+ + Br_2^{2+}$ pair in the first step.

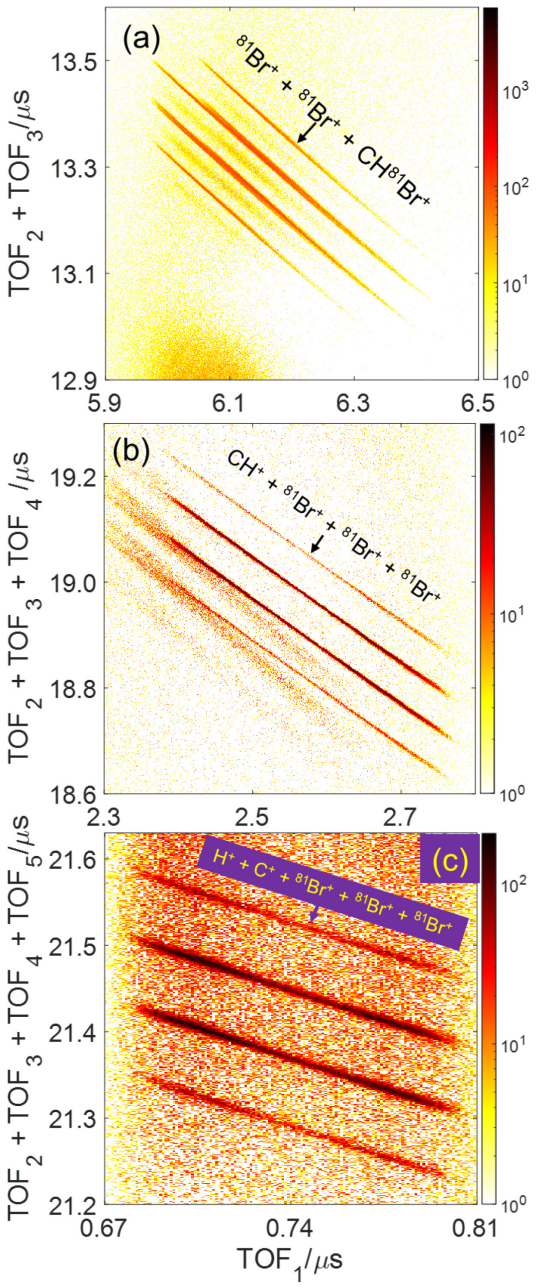

Figure 1. Three-, four-, and five-fold photoion coincidence plots of strong-field ionized $CHBr_3$ after subtraction of random coincidences, zoomed into the region of interest for the (a) $Br^+ + Br^+ + CHBr^+$, (b) $CH^+ + Br^+ + Br^+ + Br^+$, and (c) $H^+ + C^+ + Br^+ + Br^+ + Br^+$ channels. The full coincidence plots are shown in Supporting **Figures S2, S5** and **S7** in the Supporting information.

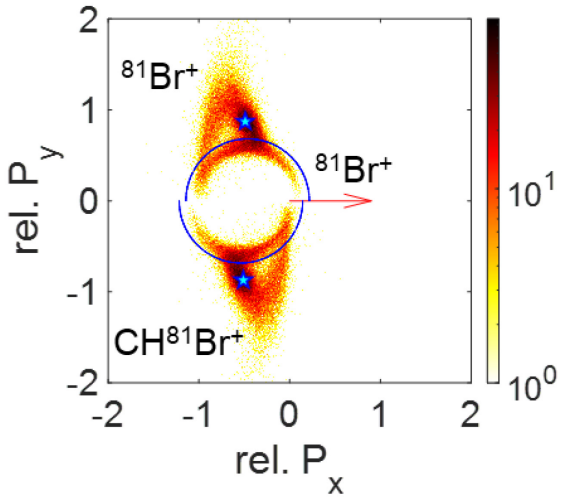

Figure 2. Newton plot of the $^{81}Br^+ + {}^{81}Br^+ + CH^{81}Br^+$ fragmentation channel measured in coincidence, showing the momentum correlation between the fragment ions. The momentum of one of the Br^+ fragments is pointing to the right (red arrow), and the normalized momenta of the other Br^+ and the $CHBr^+$ fragment ions are plotted in the upper and lower half, respectively. The blue stars and semi-circles are the momentum correlations obtained from a Coulomb explosion simulation for concerted and sequential breakup, respectively (see text).

The localized maxima on the other hand are signatures of synchronous concerted breakup.[50-51] In order to confirm these assignments, we have modeled the synchronous concerted Coulomb explosion of $CHBr_3$ initially in its equilibrium geometry assuming the classic Coulomb repulsion of point charges (see Methods). Even though such modeling is known to substantially overestimate the KER of the fragmentation process (as shown by the dashed vertical lines in **Figures S3, S6,** and **S8**), the normalized fragment momenta obtained from this model, shown as blue stars, are in excellent agreement with the position of the maxima observed in the experimental data. Similarly, modeling of a sequential breakup (shown as blue circles), in which the intermediate $CHBr_2^{2+}$ fragment breaks 50 picoseconds after the first bond breaks, and assuming a fully random orientation of the second breakup direction with respect to the first ejected Br^+ ion, reproduces the circular structures quite well.

It has been shown that in some cases, the momentum correlation in a concerted three-body breakup was able to distinguish between the distinct molecular geometries of certain structural isomers and molecular conformers.[7, 9-10] However, this is not the case for *iso*-$CHBr_3$ (as shown in **Figure S4**), and therefore, we focus on Coulomb explosion into four and five fragments next.

Since the momentum vectors of four or five fragments are, in general, not contained within a single fragmentation plane, one way of representing the momentum correlations are in the form of a three-dimensional "molecular-frame" scatter plot, as shown for the four-body channel in **Figure 3a** and for the five-body channel in **Figure 3b**. In these plots, the momentum vector of each of the detected ions is plotted with respect to the emission direction of one of the ions (CH^+ in **Figure 3a** and C^+ in **Figure 3b**), which is chosen as reference and oriented along the x-axis. Furthermore, each coincidence event is rotated such that the sum of the momentum vectors of the last two detected Br^+ ions lies in the xy-plane with positive P_y values. The resulting 3-D momentum correlation exhibits a strong visual resemblance to the nearly tetrahedral geometry of the parent molecule shown in the inset in **Figure 3a**. The momentum correlations can also be visualized by plotting the projections of the three-dimensional momentum distributions onto the three perpendicular Cartesian planes, as done in **Figures 4 and 5(a)-(c)** for the four- and five-body channels, respectively. Each of these projections shows pronounced and well-localized maxima, which we assign to fragments produced by a synchronous concerted breakup of the parent ion. In the four-body case, weaker and more diffuse curved structures resemble the

signature of sequential fragmentation in the Newton plots for three-body breakup (see **Figure 2**).[26, 28, 43-46] When plotting the same projections of the four-body channel only for those events where the KEs of each of the three $^{81}Br^+$ fragment ions is greater than 3.3 eV, i.e., excluding the small low-energy peak observed in the $^{81}Br^+$ KE distribution in **Figure S6**, only the three localized maxima remain, as shown in **Figure S10**. This further corroborates our tentative assignment of the faint curved structures to sequential fragmentation events, although further investigations of the four-body sequential fragmentation dynamics would be needed to unambiguously confirm this assignment. We note, however, that these diffuse structures are absent in the plots for five-body fragmentation in **Figure 5**, suggesting that five-body breakup is primarily concerted. This is consistent with the intuitive expectation that the likelihood of forming long-lived metastable di-cations would decrease if the total charge of the molecule increases.

Another noteworthy peculiarity in the five-body fragmentation is the extremely small relative momentum of the H^+ ion. For two- and three-body fragmentation, momentum conservation usually results in H^+ ions with a momentum that is comparable in magnitude to the other fragments, but this is not the case for five-body fragmentation, where momentum conservation does not require equal momentum of all particles. This observation is in agreement with the results of Pitzer *et al.* for five-body fragmentation of CHBrClF,[6] and also in agreement with the results of our Coulomb explosion simulations, which are shown as blue stars in **Figures 4** and **5(a)-(c).** Despite the fact that these simulations overestimate the total KER and the individual fragment KEs considerably, as shown in **Figures S6** and **S8**, these simulations and the experiment are in excellent agreement with respect to the angular momentum correlations, as already noted in the three-body case.

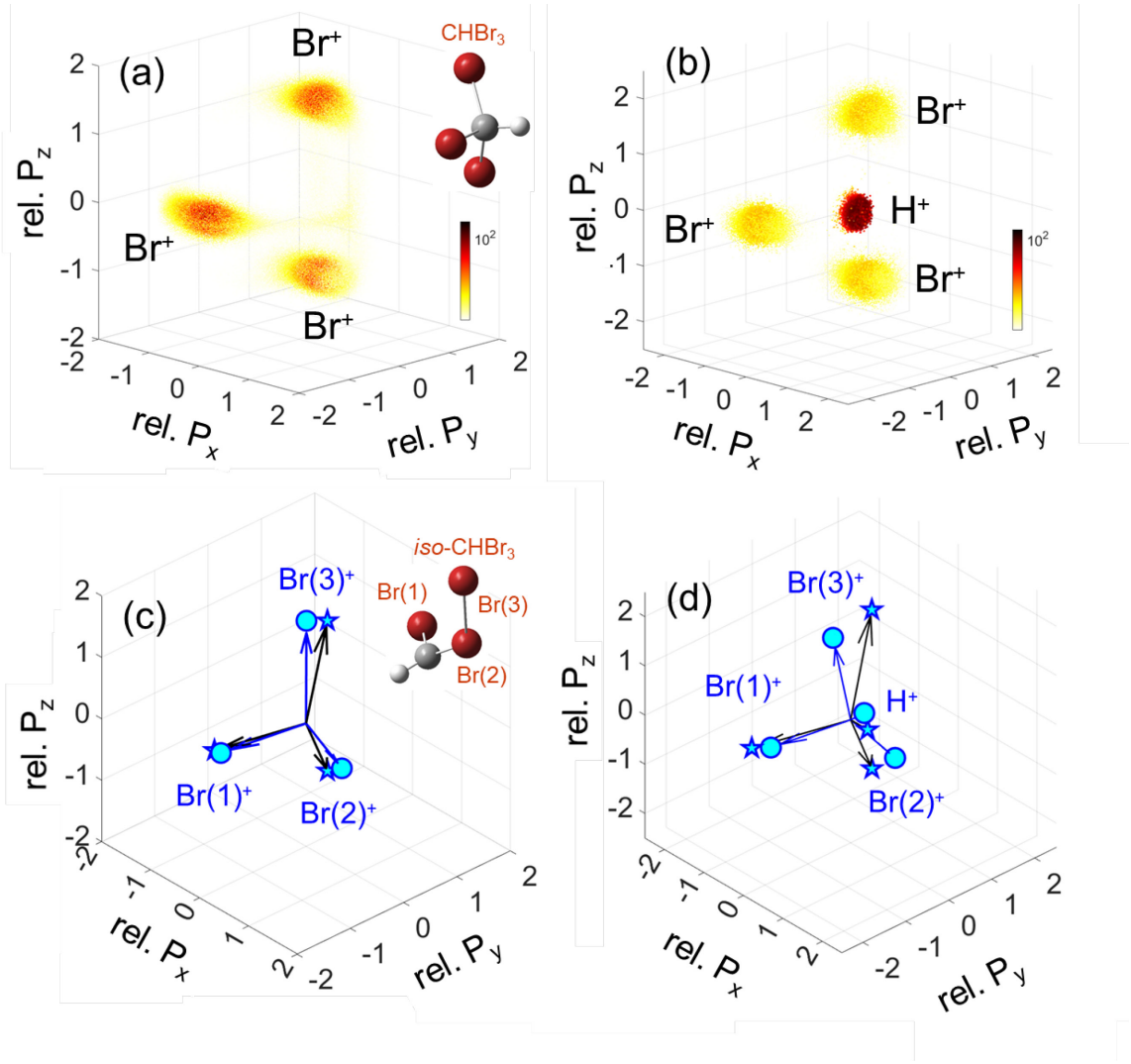

Figure 3. Three-dimensional momentum correlation plot of the (a) four-body $CH^+ + {}^{81}Br^+ + {}^{81}Br^+ + {}^{81}Br^+$ and (b) the five-body $H^+ + C^+ + {}^{81}Br^+ + {}^{81}Br^+ + {}^{81}Br^+$ channel. The momentum vectors of each fragment in a four- or five-fold coincidence event are rotated such that the momentum of the reference ion, CH^+ in (a) and C^+ in (b), points along the x-axis, and the sum of the momentum vectors of the last two detected Br^+ ions lies in the xy-plane with positive P_y values. The momenta of the remaining fragments, normalized to the magnitude of the momentum of the reference ion, are then plotted in this coordinate frame. (c, d) Coulomb explosion simulations for the equilibrium geometry of $CHBr_3$ (stars) compared to those for the equilibrium geometry of *iso*-$CHBr_3$ (circles). The two geometries are shown as insets. The reference ion and the xy-plane are defined as in **panels (a) and (c)**, and the plots are defined such that the momentum vector of the Br^+ ion marked as '1' lies in the xy-plane. Plots where ions '2' or '3' lie in the xy-plane are shown in Figs. S11.

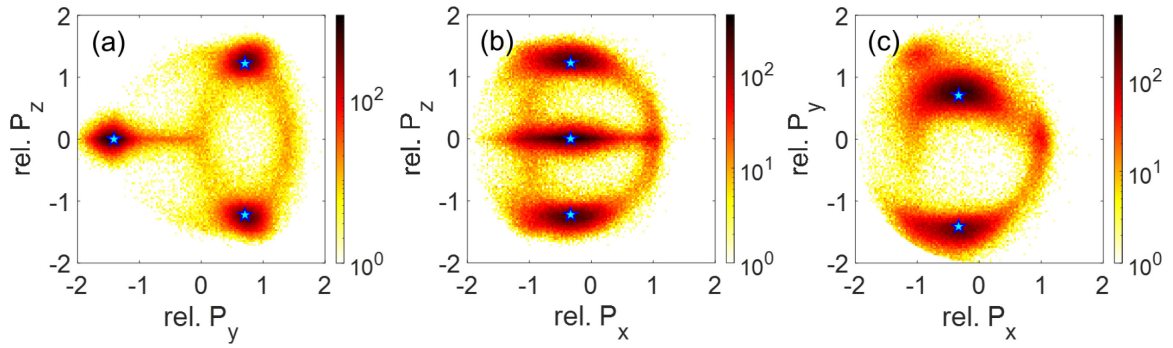

Figure 4. Projections of the distribution of the three Br^+ ions in the four-body channel shown in Figure 3(a) on the (a) yz, (b) xz, and (c) xy planes. The blue stars indicate the normalized momenta obtained from the Coulomb explosion simulations for the equilibrium geometry of the $CHBr_3$ ground state (see Methods). Coulomb explosion simulations for the isomer geometry are shown in Figure S12.

The good agreement between simulations and experiment in terms of momentum correlations allows us to further extend these simulations in order to investigate to what extent the four- and five-body fragmentation patterns can be used to distinguish between $CHBr_3$ and the *iso*-$CHBr_3$ geometry. To that end, we have performed identical simulations for the equilibrium geometry of *iso*-$CHBr_3$, whose results are shown as blue circles in **Figure 3(c)** and **(d)**. Despite the isomer geometry, shown as an inset in **Figure 3(c)**, being very different from that of the $CHBr_3$ ground state, the resulting fragment ion momentum correlations are surprisingly similar. This suggests that the qualitative features of the momentum correlation are predominantly a rather generic signature of the Coulomb repulsion between 4 or 5 positive charges. Nonetheless, closer inspection reveals clear quantitative differences, both in terms of the fragments' KEs (see **Table S1**) and momentum correlations, which are most pronounced in the five-body fragmentation shown in **Figure 3(d)**. These differences can also be seen in the projections of the 3-dimensional momentum correlations in **Figure 5**.

For a more realistic comparison with the experimental data, **Figure 5(d)-(i)** shows the Coulomb explosion simulations for five-body fragmentation of an ensemble of initial geometries representing the Wigner distribution of ground-state $CHBr_3$ and *iso*-$CHBr_3$ at a temperature of 60 K, which we estimate to be the temperature of our molecular beam. For $CHBr_3$, the simulated momentum correlations display significantly more localized maxima than what is observed experimentally, and even simulations performed for an ensemble at 300 K show only a barely visible increase of the width of each peak. This difference between experiment and simulation may be due to shortcomings of our classical point-

charge-model and also due to vibrational "heating" of the molecules during the strong infrared pulse, e.g., via Raman excitations, or to deformation of the molecules during the ionization process. However, since our main focus here lies on the possibility of distinguishing the two isomers, the most noteworthy observation when inspecting **Figure 5** is the pronounced difference of the simulated momentum correlations for $CHBr_3$ and *iso*-$CHBr_3$. The predicted positions of the maxima for *iso*-$CHBr_3$ are clearly offset from both the experimentally observed and simulated maxima for ground-state $CHBr_3$, and the distributions of the former extend deeply into regions of the Newton plots that are essentially empty in the experimental distributions. We therefore conclude that there is no indication of the formation of the isomer geometry in the current data, most likely since there is simply not enough time for the necessary nuclear re-arrangement to occur during the NIR pulse before the molecule explodes as a result of the ultrafast 4- and 5-fold ionization process. However, our simulations also suggest that the presence of *iso*-$CHBr_3$ created, e.g., by the pump pulse in a pump-probe experiment, would result in a distinct shift in the momentum correlation patterns that should be discernible in appropriate difference plots. In this context, it is important to note that since the three Br atoms in *iso*-$CHBr_3$ are no longer equivalent, three different correlation plots can be made, depending on which two of the three Br^+ ions are used to define the xy-plane. For brevity's sake, only one of these options is shown in **Figure 5** while the other two are shown in **Figure S13**, but each of them is markedly different from the simulations for $CHBr_3$.

Furthermore, our simulations also predict distinct differences in the fragment ions' KEs (**Table S1)** of $CHBr_3$ and *iso*-$CHBr_3$. In particular, the KE of the 'central' Br atom in *iso*-$CHBr_3$, labeled Br(2) in **Figures 5** and **6,** is found to be 4.0 and 4.2 eV in four- and five-body fragmentation processes, respectively. These KE values are 2.0 to 3.2 eV lower than those of the Br^+ ions in $CHBr_3$ for the respective four- and five-body fragmentations. This may allow for some additional gating on the Br^+ KEs in order to help with distinguishing *iso*-$CHBr_3$ from $CHBr_3$ in a time-resolved experiment.

In conclusion, we investigated the fragmentation of $CHBr_3$ following three-, four- and five-fold ionization induced by a strong NIR laser pulse from a tabletop laser by coincidence ion momentum imaging. Although classical simulations significantly overestimate the magnitude of the ion momenta and, thus, their KEs, excellent agreement is found in a normalized momentum correlation (Newton plot) representation, highlighting the usefulness of these momentum correlation plots for Coulomb explosion

imaging with four and five ionic fragments. Simulating the fragmentation of *iso*-$CHBr_3$, which is thought to be produced, e.g., after ultraviolet photoexcitation, we show that the isomer geometry leads to quantitative differences in the momentum correlations. We thus propose that time-resolved Coulomb-explosion-imaging experiments detecting four or five fragment ions in coincidence should be well suited to study the ultrafast formation of transient molecular structures after photoexcitation of small polyatomic molecules.

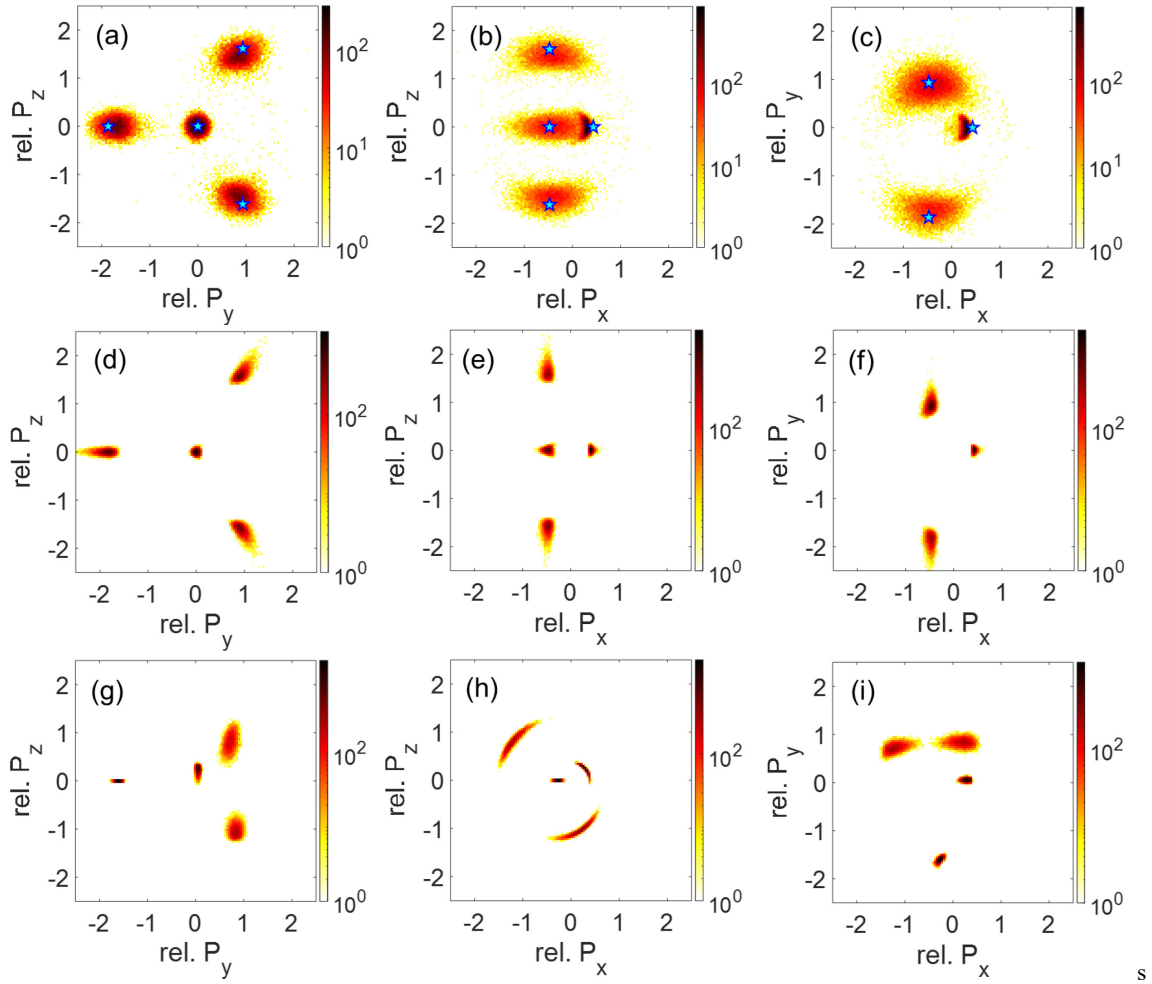

Figure 5. Projections of the experimentally obtained momentum correlation of H^+ and three $^{81}Br^+$ ions in the five-body channel shown in Fig. 3(b) on the (a) yz, (b) xz, and (c) xy planes. The blue stars indicate the normalized momenta obtained from the Coulomb explosion simulations for the initial equilibrium geometry of the $CHBr_3$ ground state. Note that the distributions of the two Br^+ ions with positive momenta along the y-directions overlap almost completely in (c), and that the two stars representing the simulated momenta of the two Br^+ ions with positive y-momentum are in identical positions. The two rows below show the same projections obtained from the Coulomb explosion simulations of ten thousand $CHBr_3$ (panels d-f) and *iso*-$CHBr_3$ (panels g-i) geometries sampling the Wigner distribution of the ground-state molecules at 60 K. Similar to Fig. 3, the plots are defined such that the momentum vector of the Br^+ ion marked as '1' lies in the xy-plane. Plots where ions '2' or '3' lie in the xy-plane are shown in Fig. S13.

Methods

EXPERIMENTAL METHODS

The linearly polarized output of an amplified Ti:Sapphire laser with a repetition rate of 10 kHz, a central wavelength of 790 nm (FWHM 60 nm), and a pulse duration of 28 fs in the interaction region (as determined by an independent frequency-resolved optical gating (FROG) measurement), was focused into a supersonic molecular beam by a spherical concave mirror with a focal length of 75 mm. The data shown here were recorded with a pulse energy of 13 μJ, which resulted in a peak intensity of 6×10^{14} Wcm^{-2} in the interaction region, according to calibration measurement using the well-known recoil momentum profile of strong-field ionized neon atoms.[52] The intense laser pulses interacted with $CHBr_3$ introduced as a supersonic molecular beam into the center of a COLd Target Recoil Ion Momentum Spectrometer (COLTRIMS).[21, 53-54] The ions produced in the interaction were accelerated by applying a uniform extraction field of 96.6 V cm^{-1} along a 240 mm long spectrometer towards a Z-stacked microchannel plate (MCP) detector equipped with an 80-mm time- and position-sensitive delay-line anode. We recently upgraded our detector with efficiency enhanced "funnel MCPs", which significantly increase the detection efficiency up to a reported 90%,[55] thus increasing the total rate of five-fold ion coincidences by more than one order of magnitude compared to previous MCPs. The data shown here were acquired for 21 hours, and **Figures 3** and **4** contain 62K and 9K coincidence events, respectively.

For this experiment, triboromethane (99%), $CHBr_3$, purchased from Sigma Aldrich, was used without further purification. Approximately 10 ml of $CHBr_3$ was put into a stainless-steel gas bubbler, subjected to several freeze-pump-thaw cycles in order to minimize contamination by atmospheric gases, and then expanded into the ultra-high vacuum through a 30-μm diameter flat nozzle at room temperature using helium (He) at 250 Torr as a carrier gas. We analyze only the ^{81}Br isotopic channel for all the fragmentation channels discussed here. However, since the small mass difference between the two Br isotopes has only a very minor influence on the Coulomb explosion process (see **Figure S9**), the results for all four isotope combinations could, in principle, be combined to obtain more than eight times as many events for four- and five-body breakup processes, which could be statistically crucial for a pump-

probe experiment. Since the present data set has sufficient statistics, we restricted the analysis to the pure ^{81}Br isotopic channels, which are separated the most from any background contributions.

COULOMB EXPLOSION SIMULATIONS

Under the simplifying assumption that the interaction is purely governed by Coulomb repulsion between point charges and that there is no energy stored in the internal degrees of freedom of the fragments, one can estimate the KER and KE of the individual ionic fragments produced from the ionic *n*-body fragmentation of the parent molecule and obtain their momenta at any given time during the fragmentation by numerically solving the classical equations of motion of *n* point charges under the influence of the Coulomb field. To assess how well such a simple model can reproduce the experimentally observed KERs and momentum correlations, such a Coulomb explosion simulation was performed for the ground state geometry of the $CHBr_3$ parent and the *iso*-$CHBr_3$ molecules. Both the molecules are optimized at the B3LYP/aug-cc-pVDZ level of theory without any constraints. For simulating the three-body fragmentation, unit charges were placed on the three bromine atoms. For the four-body fragmentation, unit charges were placed on the carbon and the three bromine atoms. Unit point charges were placed on all individual atoms for five-body fragmentation simulation.

ASSOCIATED CONTENT

Supporting Information

Ion time-of-flight spectrum; kinetic energy release, full multi-ion coincidence plots, momentum correlation plots, additional Coulomb explosion simulation results.

Acknowledgments

We gratefully acknowledge the technical staff of JRML for support during the preparation of the experiment. We also acknowledge Max Sayler and other former members of Itzik Ben-Itzhak's group for the development of the computer code to reconstruct lost delay-line signals, which was implemented in the data analysis for this paper. This work was supported primarily by the Chemical Sciences,

Geosciences, and Biosciences Division, Office of Basic Energy Sciences, Office of Science, US Department of Energy, Grant No. DEFG02-86ER13491. S.B. was supported by Grant No. DE-SC0020276; K.B. and E.W. by Grant No. DE-SC0019451; and the PULSAR laser was provided by Grant No. DE-FG02-09ER16115 from the same funding agency. N.M. was supported by the National Science Foundation (NSF) Grant No. PHYS-1753324 to D.R.

References

(1) Vager, Z.; Naaman, R.; Kanter, E. P. Coulomb Explosion Imaging of Small Molecules. *Science* **1989**, *244* (4903), 426-431.
(2) Kanter, E. P.; Vager, Z.; Both, G.; Zajfman, D. A Measurement of the Low Energy Stereostructure of Protonated Acetylene, $C_2H_3^+$. *J. Chem. Phys.* **1986**, *85* (12), 7487-7488.
(3) Vager; Kanter; Both; Cooney; Faibis; Koenig; Zabransky; Zajfman. Direct Determination of the Stereochemical Structure of CH_4^+. *Phys. Rev. Lett.* **1986**, *57* (22), 2793-2795.
(4) Vager, Z.; Zajfman, D.; Graber, T.; Kanter, E. P. Experimental Evidence for Anomalous Nuclear Delocalization in $C_2H_3^+$. *Phys. Rev. Lett.* **1993**, *71* (26), 4319-4322.
(5) Zajfman, D.; Vager, Z.; Naaman, R.; Mitchell, R. E.; Kanter, E. P.; Graber, T.; Belkacem, A. The Structures of C2H+ and C2H+2 as Measured by Coulomb Explosion Imaging. *J. Chem. Phys.* **1991**, *94* (10), 6377-6387.
(6) Pitzer, M.; Kunitski, M.; Johnson, A. S.; Jahnke, T.; Sann, H.; Sturm, F.; Schmidt, L. P. H.; Schmidt-Böcking, H.; Dörner, R.; Stohner, J.; Kiedrowski, J.; Reggelin, M.; Marquardt, S.; Schießer, A.; Berger, R.; Schöffler, M. S. Direct Determination of Absolute Molecular Stereochemistry in Gas Phase by Coulomb Explosion Imaging. *Science* **2013**, 341 (6150), 1096-1100.
(7) Ablikim, U.; Bomme, C.; Osipov, T.; Xiong, H.; Obaid, R.; Bilodeau, R. C.; Kling, N. G.; Dumitriu, I.; Augustin, S.; Pathak, S.; Schnorr, K.; Kilcoyne, D.; Berrah, N.; Rolles, D. A Coincidence Velocity Map Imaging Spectrometer for Ions and High-energy Electrons to Study Inner-shell Photoionization of Gas-phase Molecules. *Rev. Sci. Instrum.* **2019**, *90* (5), 055103.
(8) Ablikim, U.; Bomme, C.; Savelyev, E.; Xiong, H.; Kushawaha, R.; Boll, R.; Amini, K.; Osipov, T.; Kilcoyne, D.; Rudenko, A.; Berrah, N.; Rolles, D. Isomer-dependent Fragmentation Dynamics of Inner-shell Photoionized Difluoroiodobenzene. *Phys. Chem. Chem. Phys.* **2017**, *19* (21), 13419-13431.
(9) Ablikim, U.; Bomme, C.; Xiong, H.; Savelyev, E.; Obaid, R.; Kaderiya, B.; Augustin, S.; Schnorr, K.; Dumitriu, I.; Osipov, T.; Bilodeau, R.; Kilcoyne, D.; Kumarappan, V.; Rudenko, A.; Berrah, N.; Rolles, D. Identification of Absolute Geometries of cis and trans Molecular Isomers by Coulomb Explosion Imaging. *Sci. Rep.* **2016**, *6* (1), 38202.
(10) Pathak, S.; Obaid, R.; Bhattacharyya, S.; Burger, J.; Li, X.; Tross, J.; Severt, T.; Davis, B.; Bilodeau, R. C.; Trallero-Herrero, C. A.; Rudenko, A.; Berrah, N.; Rolles, D. Differentiating and Quantifying Gas-Phase Conformational Isomers Using Coulomb Explosion Imaging. *J. Phys. Chem. Lett.* **2020**, *11* (23), 10205-10211.
(11) Stapelfeldt, H.; Constant, E.; Sakai, H.; Corkum, P. B. Time-resolved Coulomb Explosion imaging: A Method to Measure Structure and Dynamics of Molecular Nuclear Wave Packets. *Phys. Rev. A* **1998**, *58* (1), 426-433.
(12) Christensen, L.; Nielsen, J. H.; Brandt, C. B.; Madsen, C. B.; Madsen, L. B.; Slater, C. S.; Lauer, A.; Brouard, M.; Johansson, M. P.; Shepperson, B.; Stapelfeldt, H. Dynamic Stark Control of Torsional Motion by a Pair of Laser Pulses. *Phys. Rev. Lett.* **2014**, *113* (7), 073005.
(13) Christensen, L.; Nielsen, J. H.; Slater, C. S.; Lauer, A.; Brouard, M.; Stapelfeldt, H. Using Laser-induced Coulomb Explosion of Aligned Chiral Molecules to Determine their Absolute Configuration. *Phys. Rev. A* **2015**, *92* (3), 033411.

(14) Allum, F.; Burt, M.; Amini, K.; Boll, R.; Köckert, H.; Olshin, P. K.; Bari, S.; Bomme, C.; Braße, F.; Cunha de Miranda, B.; Düsterer, S.; Erk, B.; Géléoc, M.; Geneaux, R.; Gentleman, A. S.; Goldsztejn, G.; Guillemin, R.; Holland, D. M. P.; Ismail, I.; Johnsson, P.; Journel, L.; Küpper, J.; Lahl, J.; Lee, J. W. L.; Maclot, S.; Mackenzie, S. R.; Manschwetus, B.; Mereshchenko, A. S.; Mason, R.; Palaudoux, J.; Piancastelli, M. N.; Penent, F.; Rompotis, D.; Rouzée, A.; Ruchon, T.; Rudenko, A.; Savelyev, E.; Simon, M.; Schirmel, N.; Stapelfeldt, H.; Techert, S.; Travnikova, O.; Trippel, S.; Underwood, J. G.; Vallance, C.; Wiese, J.; Ziaee, F.; Brouard, M.; Marchenko, T.; Rolles, D. Coulomb Explosion Imaging of CH_3I and CH_2ClI Photodissociation Dynamics. *J. Chem. Phys.* **2018**, *149* (20), 204313.
(15) Burt, M.; Boll, R.; Lee, J. W. L.; Amini, K.; Köckert, H.; Vallance, C.; Gentleman, A. S.; Mackenzie, S. R.; Bari, S.; Bomme, C.; Düsterer, S.; Erk, B.; Manschwetus, B.; Müller, E.; Rompotis, D.; Savelyev, E.; Schirmel, N.; Techert, S.; Treusch, R.; Küpper, J.; Trippel, S.; Wiese, J.; Stapelfeldt, H.; de Miranda, B. C.; Guillemin, R.; Ismail, I.; Journel, L.; Marchenko, T.; Palaudoux, J.; Penent, F.; Piancastelli, M. N.; Simon, M.; Travnikova, O.; Brausse, F.; Goldsztejn, G.; Rouzée, A.; Géléoc, M.; Geneaux, R.; Ruchon, T.; Underwood, J.; Holland, D. M. P.; Mereshchenko, A. S.; Olshin, P. K.; Johnsson, P.; Maclot, S.; Lahl, J.; Rudenko, A.; Ziaee, F.; Brouard, M.; Rolles, D. Coulomb-explosion Imaging of Concurrent CH_2BrI Photodissociation Dynamics. *Phys. Rev. A* **2017**, *96* (4), 043415.
(16) Luo, S.; Hu, W.; Yu, J.; Li, X.; He, L.; Wang, C.; Liu, F.; Ding, D. Multielectron Effects in the Strong Field Sequential Ionization of Aligned CH_3I Molecules. *J. Phys. Chem. A* **2017**, *121* (35), 6547-6553.
(17) Luo, S.; Zhou, S.; Hu, W.; Yu, J.; Li, X.; Ma, P.; He, L.; Wang, C.; Guo, F.; Yang, Y.; Ding, D. Identifying the Multielectron Effect on Chemical Bond Rearrangement of CH_3Cl Molecules in Strong Laser Fields. *J. Phys. Chem. A* **2018**, *122* (43), 8427-8432.
(18) Yu, X.; Zhao, X.; Wang, Z.; Yang, Y.; Zhang, X.; Ma, P.; Li, X.; Wang, C.; Xu, X.; Wang, C.; Zhang, D.; Luo, S.; Ding, D. Determining the Stereo Configuration of Carbonyl Sulfide Dimers using Coulomb-explosion Imaging. *Phys. Rev. A* **2021**, *104* (5), 053104.
(19) Voigtsberger, J.; Zeller, S.; Becht, J.; Neumann, N.; Sturm, F.; Kim, H. K.; Waitz, M.; Trinter, F.; Kunitski, M.; Kalinin, A.; Wu, J.; Schöllkopf, W.; Bressanini, D.; Czasch, A.; Williams, J. B.; Ullmann-Pfleger, K.; Schmidt, L. P. H.; Schöffler, M. S.; Grisenti, R. E.; Jahnke, T.; Dörner, R. Imaging the Structure of the Trimer Systems $^4He_3$ and $^3He^4He_2$. *Nat. Commun.* **2014**, 5 (1), 5765.
(20) Dorn, A.; Kheifets, A.; Schröter, C. D.; Najjari, B.; Höhr, C.; Moshammer, R.; Ullrich, J. Double Ionization of Helium by Electron-Impact: Complete Pictures of the Four-Body Breakup Dynamics. *Phys. Rev. Lett.* **2001**, *86* (17), 3755-3758.
(21) Malakar, Y.; Pearson, W. L.; Zohrabi, M.; Kaderiya, B.; Raju, P. K.; Ziaee, F.; Xue, S.; Le, A. T.; Ben-Itzhak, I.; Rolles, D.; Rudenko, A. Time-resolved Imaging of Bound and Dissociating Nuclear Wave Packets in Strong-field Ionized Iodomethane. *Phys. Chem. Chem. Phys.* **2019**, *21* (26), 14090-14102.
(22) Ergler, T.; Rudenko, A.; Feuerstein, B.; Zrost, K.; Schröter, C. D.; Moshammer, R.; Ullrich, J. Spatiotemporal Imaging of Ultrafast Molecular Motion: Collapse and Revival of the D_2+ Nuclear Wave Packet. *Phys. Rev. Lett.* **2006**, *97* (19), 193001.
(23) Endo, T.; Neville, S. P.; Wanie, V.; Beaulieu, S.; Qu, C.; Deschamps, J.; Lassonde, P.; Schmidt, B. E.; Fujise, H.; Fushitani, M.; Hishikawa, A.; Houston, P. L.; Bowman, J. M.; Schuurman, M. S.; Légaré, F.; Ibrahim, H. Capturing Roaming Molecular Fragments in Real Time. *Science* **2020**, *370* (6520), 1072-1077.
(24) Allum, F.; Anders, N.; Brouard, M.; Bucksbaum, P.; Burt, M.; Downes-Ward, B.; Grundmann, S.; Harries, J.; Ishimura, Y.; Iwayama, H.; Kaiser, L.; Kukk, E.; Lee, J.; Liu, X.; Minns, R. S.; Nagaya, K.; Niozu, A.; Niskanen, J.; O'Neal, J.; Owada, S.; Pickering, J.; Rolles, D.; Rudenko, A.; Saito, S.; Ueda, K.; Vallance, C.; Werby, N.; Woodhouse, J.; You, D.; Ziaee, F.; Driver, T.; Forbes, R. Multi-channel Photodissociation and XUV-induced Charge Transfer Dynamics in Strong-field-ionized Methyl Iodide Studied with Time-resolved Recoil-frame Covariance Imaging. *Faraday Discuss.* **2021**, *228*, 571-596.
(25) Forbes, R.; Allum, F.; Bari, S.; Boll, R.; Borne, K.; Brouard, M.; Bucksbaum, P. H.; Ekanayake, N.; Erk, B.; Howard, A. J.; Johnsson, P.; Lee, J. W. L.; Manschwetus, B.; Mason, R.; Passow, C.; Peschel, J.; Rivas, D. E.; Rörig, A.; Rouzée, A.; Vallance, C.; Ziaee, F.; Rolles, D.; Burt,

M. Time-resolved Site-Selective Imaging of Predissociation and Charge Transfer Dynamics: the CH_3I B-band. *J. Phys. B: At. Mol. Opt. Phys.* **2020**, 53 (22), 224001.
(26) Wang, E.; Shan, X.; Shen, Z.; Gong, M.; Tang, Y.; Chen, X. Fragmentation Dynamics of Nitrogen Trifluoride Induced by Electron Collision. *J. Chem. Phys.* **2019**, *151* (13), 134308.
(27) Eland, J. H. D. The Dynamics of Three-body Dissociations of Dications Studied by the Triple Coincidence Technique PEPIPICO. *Mol. Phys.* **1987**, *61* (3), 725-745.
(28) Hsieh, S.; Eland, J. H. D. Reaction Dynamics of Three-body Dissociations in Triatomic Molecules from Single-photon Double Ionization Studied by a Time- and Position-sensitive Coincidence Method. *J. Phys. B: At. Mol. Opt. Phys.* **1997**, *30* (20), 4515-4534
(29. Wang, B.; Han, J.; Zhu, X.; Wei, L.; Ren, B.; Zhang, Y.; Yu, W.; Yan, S.; Ma, X.; Zou, Y.; Chen, L.; Wei, B. Dissociative Ionization of OCS Induced by Highly Charged Ion Impact. *Phys. Rev. A* **2021**, *103* (4), 042810.
(30) Luzon, I.; Livshits, E.; Gope, K.; Baer, R.; Strasser, D. Making Sense of Coulomb Explosion Imaging. *J. Phys. Chem. Lett.* **2019**, *10* (6), 1361-1367.
(31) Erk, B.; Rolles, D.; Foucar, L.; Rudek, B.; Epp, S. W.; Cryle, M.; Bostedt, C.; Schorb, S.; Bozek, J.; Rouzee, A.; Hundertmark, A.; Marchenko, T.; Simon, M.; Filsinger, F.; Christensen, L.; De, S.; Trippel, S.; Küpper, J.; Stapelfeldt, H.; Wada, S.; Ueda, K.; Swiggers, M.; Messerschmidt, M.; Schröter, C. D.; Moshammer, R.; Schlichting, I.; Ullrich, J.; Rudenko, A. Ultrafast Charge Rearrangement and Nuclear Dynamics upon Inner-Shell Multiple Ionization of Small Polyatomic Molecules. *Phys. Rev. Lett.* **2013**, *110* (5), 053003.
(32) Sayler, A. M.; Eckner, E.; McKenna, J.; Esry, B. D.; Carnes, K. D.; Ben-Itzhak, I.; Paulus, G. G. Nonunique and Nonuniform Mapping in Few-body Coulomb-explosion Imaging. *Phys. Rev. A* **2018**, *97* (3), 033412.
(33) Herwig, P.; Zawatzky, K.; Grieser, M.; Heber, O.; Jordon-Thaden, B.; Krantz, C.; Novotný, O.; Repnow, R.; Schurig, V.; Schwalm, D.; Vager, Z.; Wolf, A.; Trapp, O.; Kreckel, H. Imaging the Absolute Configuration of a Chiral Epoxide in the Gas Phase. *Science* **2013**, *342* (6162), 1084-1086.
(34) Pitzer, M.; Kastirke, G.; Kunitski, M.; Jahnke, T.; Bauer, T.; Goihl, C.; Trinter, F.; Schober, C.; Henrichs, K.; Becht, J.; Zeller, S.; Gassert, H.; Waitz, M.; Kuhlins, A.; Sann, H.; Sturm, F.; Wiegandt, F.; Wallauer, R.; Schmidt, L. P. H.; Johnson, A. S.; Mazenauer, M.; Spenger, B.; Marquardt, S.; Marquardt, S.; Schmidt-Böcking, H.; Stohner, J.; Dörner, R.; Schöffler, M.; Berger, R. Absolute Configuration from Different Multifragmentation Pathways in Light-Induced Coulomb Explosion Imaging. *Chem. Phys. Chem.* **2016**, *17* (16), 2465-2472.
(35) Pitzer, M.; Kastirke, G.; Burzynski, P.; Weller, M.; Metz, D.; Neff, J.; Waitz, M.; Trinter, F.; Schmidt, L. P. H.; Williams, J. B.; Jahnke, T.; Schmidt-Bocking, H.; Berger, R.; Dorner, R.; Schoffler, M. Stereochemical Configuration and Selective Excitation of the Chiral Molecule Halothane. *J. Phys. B: At. Mol. Opt. Phys.* **2016**, *49* (23), 234001.
(36) Tseng, C.-M.; Fushitani, M.; Matsuda, A.; Hishikawa, A. Coincidence Momentum Imaging of Four- and Three-body Coulomb Explosion of Formaldehyde in Ultrashort Intense Laser Fields. *J. Electron Spectrosc. Relat. Phenom.* **2018**, *228*, 25-30.
(37) Li, X.; Rudenko, A.; Schöffler, M. S.; Anders, N.; Baumann, T. M.; Eckart, S.; Erk, B.; De Fanis, A.; Fehre, K.; Dörner, R.; Foucar, L.; Grundmann, S.; Grychtol, P.; Hartung, A.; Hofmann, M.; Ilchen, M.; Janke, C.; Kastirke, G.; Kircher, M.; Kubicek, K.; Kunitski, M.; Mazza, T.; Meister, S.; Melzer, N.; Montano, J.; Music, V.; Nalin, G.; Ovcharenko, Y.; Passow, C.; Pier, A.; Rennhack, N.; Rist, J.; Rivas, D. E.; Schlichting, I.; Schmidt, L. P. H.; Schmidt, P.; Siebert, J.; Strenger, N.; Trabert, D.; Trinter, F.; Vela-Perez, I.; Wagner, R.; Walter, P.; Weller, M.; Ziolkowski, P.; Czasch, A.; Rolles, D.; Meyer, M.; Jahnke, T.; Boll, R. Coulomb Explosion Imaging of Small Polyatomic Molecules with Ultrashort X-ray Pulses. *Phys. Rev. Res.* **2022**, *4* (1), 013029.
(38) Boll, R.; Schäfer, J. M.; Richard, B.; Fehre, K.; Kastirke, G.; Jurek, Z.; Schöffler, M. S.; Abdullah, M. M.; Anders, N.; Baumann, T. M.; Eckart, S.; Erk, B.; De Fanis, A.; Dörner, R.; Grundmann, S.; Grychtol, P.; Hartung, A.; Hofmann, M.; Ilchen, M.; Inhester, L.; Janke, C.; Jin, R.; Kircher, M.; Kubicek, K.; Kunitski, M.; Li, X.; Mazza, T.; Meister, S.; Melzer, N.; Montano, J.; Music, V.; Nalin, G.; Ovcharenko, Y.; Passow, C.; Pier, A.; Rennhack, N.; Rist, J.; Rivas, D. E.; Rolles, D.; Schlichting, I.; Schmidt, L. P. H.; Schmidt, P.; Siebert, J.; Strenger, N.; Trabert, D.; Trinter, F.; Vela-Perez, I.; Wagner, R.; Walter, P.; Weller, M.; Ziolkowski, P.; Son, S.-K.; Rudenko,

A.; Meyer, M.; Santra, R.; Jahnke, T. X-ray Multiphoton-induced Coulomb Explosion Images Complex Single Molecules. *Nat. Phys.* **2022**, *18*, 423-428.
(39) Mereshchenko, A. S.; Butaeva, E. V.; Borin, V. A.; Eyzips, A.; Tarnovsky, A. N. Roaming-mediated Ultrafast Isomerization of Geminal Tri-bromides in the Gas and Liquid Phases. *Nat. Chem.* **2015**, *7* (7), 562-568.
(40) Pal, S. K.; Mereshchenko, A. S.; Butaeva, E. V.; El-Khoury, P. Z.; Tarnovsky, A. N. Global Sampling of the Photochemical Reaction Paths of Bromoform by Ultrafast Deep-UV through Near-IR Transient Absorption and ab initio Multiconfigurational Calculations. *J. Chem. Phys.* **2013**, *138* (12), 124501.
(41) George, L.; Kalume, A.; Esselman, B. J.; Wagner, J.; McMahon, R. J.; Reid, S. Spectroscopic and Computational Studies of Matrix-isolated *iso*-$CHBr_3$: Structure, Properties, and Photochemistry of iso Bromoform. *J. Chem. Phys.* **2011**, *135* (12), 124503.
(42) Toulson, B. W.; Borgwardt, M.; Wang, H.; Lackner, F.; Chatterley, A. S.; Pemmaraju, C. D.; Neumark, D. M.; Leone, S. R.; Prendergast, D.; Gessner, O. Probing ultrafast C-Br Bond Fission in the UV Photochemistry of Bromoform with Core-to-valence Transient Absorption Spectroscopy. Struct. Dyn. 2019, 6, 054304.
(43) Neumann, N.; Hant, D.; Schmidt, L. P. H.; Titze, J.; Jahnke, T.; Czasch, A.; Schöffler, M. S.; Kreidi, K.; Jagutzki, O.; Schmidt-Böcking, H.; Dörner, R. Fragmentation Dynamics of CO_2^{3+} Investigated by Multiple Electron Capture in Collisions with Slow Highly Charged Ions. *Phys. Rev. Lett.* **2010**, *104* (10), 103201.
(44) Guillemin, R.; Decleva, P.; Stener, M.; Bomme, C.; Marin, T.; Journel, L.; Marchenko, T.; Kushawaha, R. K.; Jänkälä, K.; Trcera, N.; Bowen, K. P.; Lindle, D. W.; Piancastelli, M. N.; Simon, M. Selecting Core-hole Localization or Delocalization in CS_2 by Photofragmentation Dynamics. *Nat. Commun.* **2015**, *6* (1), 6166.
(45) Khan, A.; Tribedi, L. C.; Misra, D. Three-body Fragmentation of Multiply Charged Nitrous Oxide Induced by Ar^{8+}- and Xe^{15+}-ion Impact. *Phys. Rev. A* **2017**, *96* (1), 012703.
(46) Khan, A.; Tribedi, L. C.; Misra, D. Observation of a Sequential Process in Charge-asymmetric Dissociation of CO_2^{q+} (q=4,5) upon the Impact of Highly Charged Ions. *Phys. Rev. A* **2015**, 92 (3), 030701.
(47) Streeter, Z. L.; Yip, F. L.; Lucchese, R. R.; Gervais, B.; Rescigno, T. N.; McCurdy, C. W. Dissociation Dynamics of the Water Dication Following One-photon Double Ionization. I. Theory. *Phys. Rev. A* **2018,** *98* (5), 053429.
(48) Cheng, C.; Streeter, Z. L.; Howard, A. J.; Spanner, M.; Lucchese, R. R.; McCurdy, C. W.; Weinacht, T.; Bucksbaum, P. H.; Forbes, R. Strong-field ionization of water. II. Electronic and Nuclear Dynamics En Route to Double Ionization. *Phys. Rev. A* **2021,** *104* (2), 023108.
(49) Corrales, M. E.; Gitzinger, G.; González-Vázquez, J.; Loriot, V.; de Nalda, R.; Bañares, L. Velocity Map Imaging and Theoretical Study of the Coulomb Explosion of CH_3I under Intense Femtosecond IR Pulses. *J. Phys. Chem. A* **2012,** *116* (11), 2669-2677.
(50) Rajput, J.; Severt, T.; Berry, B.; Jochim, B.; Feizollah, P.; Kaderiya, B.; Zohrabi, M.; Ablikim, U.; Ziaee, F.; Raju P, K.; Rolles, D.; Rudenko, A.; Carnes, K. D.; Esry, B. D.; Ben-Itzhak, I. Native Frames: Disentangling Sequential from Concerted Three-Body Fragmentation. *Phys. Rev. Lett.* **2018**, *120* (10), 103001.
(51) Maul, C.; Gericke, K. H. Photo Induced Three Body Decay. *Int. Rev. Phys. Chem.* **1997**, *16* (1), 1-79.
(52) Rudenko, A.; Zrost, K.; Schroter, C. D.; de Jesus, V. L. B.; Feuerstein, B.; Moshammer, R.; Ullrich, J. Resonant Structures in the Low-energy Electron Continuum for Single Ionization of Atoms in the Tunnelling Regime. *J. Phys. B: At. Mol. Opt. Phys.* **2004**, *37* (24), L407-L413.
(53) Maharjan, C. M. Momentum Imaging Studies of Electron and Ion dynamics in a Strong Laser Field,. PhD thesis, **2007**.
(54) Xiong, Y.; Borne, K.; Carrascosa, A. M.; Saha, S. K.; Wilkin, K. J.; Yang, M.; Bhattacharyya, S.; Chen, K.; Du, W.; Ma, L.; Marshall, N.; Nunes, J. P. F.; Pathak, S.; Phelps, Z.; Xu, X.; Yong, H.; Lopata, K.; Weber, P. M.; Rudenko, A.; Rolles, D.; Centurion, M. Strong-field Induced Fragmentation and Isomerization of Toluene Probed by Ultrafast Femtosecond Electron Diffraction and Mass Spectrometry. *Faraday Discuss.* **2021**, *228*, 39-59.

(55) Fehre, K.; Trojanowskaja, D.; Gatzke, J.; Kunitski, M.; Trinter, F.; Zeller, S.; Schmidt, L. P. H.; Stohner, J.; Berger, R.; Czasch, A.; Jagutzki, O.; Jahnke, T.; Dorner, R.; Schoffler, M. S. Absolute Ion Detection Efficiencies of Microchannel Plates and Funnel Microchannel Plates for Multi-coincidence Detection. *Rev. Sci. Instrum*. **2018**, *89* (4), 045112.